National Research University Higher School of Economics

as a manuscript

Matyushkin Iakov Evgenyevich

Asymmetric field-effect transistors based on graphene and carbon nanotubes for polarization-sensitive detection of terahertz radiation

Dissertation summary
for the purpose of obtaining academic degree
Doctor of Philosophy in Engineering

Academic supervisor:
Doctor of Physical and Mathematical Sciences
Professor
Goltsman Grigory Naumovich

Moscow – 2023

Contents

Introduction

The radiation of the terahertz, or, as it is also called, the submillimeter range occupies the region between infrared and radio waves in the electromagnetic spectrum (Fig. 1). Terahertz waves are called waves lying in the interval: 0.03 - 3 mm (0.1 - 10 THz). This region of the spectrum has attracted close attention of scientists in the last few decades [1]. Terahertz radiation has a low quantum energy (0.4 - 40 meV), is non-ionizing, easily passes through most dielectrics (wood, plastic, ceramics, paper, fabric), while it is reflected from conductive materials and is strongly absorbed by water. This set of properties makes terahertz radiation promising for various applications, in tasks:

- spectroscopy [2-6];
- spatial scanning and imaging (for example, in security systems or in the food industry) [7,8];
- ellipsometry [9,10];
- research of astronomical objects [11-15];
- telecommunications [16-18];

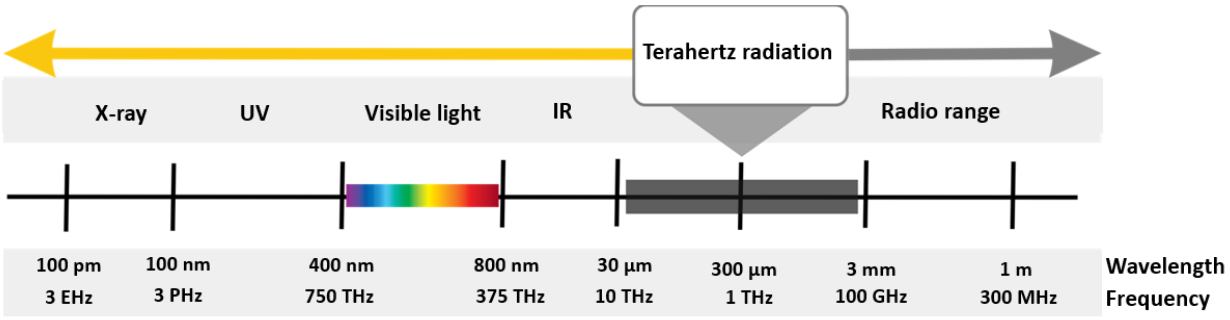

Figure 1 — Place of terahertz radiation in the electromagnetic spectrum.

Problem statement

To build devices operating in the terahertz range, efficient radiation sources and detectors are required. There are various ways to implement a terahertz detector, each of which has its own advantages and disadvantages.

For example, Golay cells (and other pyroelectric detectors) can measure radiation power, but are slow. Superconducting bolometers (HEB - hot electron bolometers) have a record high sensitivity and speed, but are able to operate exclusively at liquid helium temperatures, which makes these devices expensive and difficult to operate. Schottky diodes also have high detectivity and speed, but require cooling to liquid nitrogen temperatures (77 K), and most importantly, the detection efficiency in them drops exponentially at frequencies above 1 THz. High electron mobility transistors (HEMTs) are the most versatile devices: they also have high sensitivity and speed, but are also capable of operating at room temperatures and provide effective detection in a wide frequency range: from 100 GHz to 10 THz.

Any electromagnetic wave has four main characteristics: frequency (wavelength), amplitude, phase and polarization. Most research on terahertz detectors is aimed at improving the efficiency of detecting precisely the wave amplitude, although characteristics such as phase and polarization also carry information that can be used for applied purposes, for example, in holography and imaging, ellipsometry, spectroscopy and telecommunications.

Thus, the present work is aimed at studying the possibility of creating detectors, in the configuration of field-effect transistors, for polarization-sensitive detection of terahertz radiation. One of the promising ways to create such devices is the use of new low-dimensional materials.

The unique properties of low-dimensional materials make them attractive, including for the development of terahertz devices. In particular, it is promising to use graphene and carbon nanotubes to create sensitive, fast, low-noise and broadband terahertz radiation detectors, which has been demonstrated in a number of works. Terahertz radiation detectors based on graphene and carbon nanotubes can be created using various physical principles and radiation detection mechanisms: photovoltaic, bolometric, thermoelectric, barrier rectification, resistive self-mixing [19]. There is another mechanism, the so-called Dyakonov-

Shur straightening. This mechanism is based on the fact that the electromagnetic radiation incident on the detector is compressed into ultrashort plasma waves, which are then rectified by the nonlinearity in the device channel. This mechanism can be implemented in any systems with 2DEG (two-dimensional electron gas) and was studied in a series of works both theoretically [20, 21] and experimentally [22, 23]. It is very promising, since it provides a high efficiency of converting the electromagnetic energy incident on the detector into a useful signal and allows detection in the resonance mode. The functioning of the detectors studied in this work is described by expanding the Dyakonov-Shur hydrodynamic model [24].

Despite a large number of studies devoted to the interaction of terahertz radiation with detectors based on graphene and carbon nanotubes, the dependence of the photoresponse on the direction and type of polarization has hardly been studied. Except for a few works [25, 26], where the dependence of the photoresponse on different orientations of the linear polarization of radiation relative to THz antennas was studied. The interaction of a two-dimensional electron gas with radiation of elliptical and circular polarization was studied in [27] and showed a rather nontrivial result: a circular effect was observed - the sign of the constant photovoltage changed depending on the direction of circular polarization. However, the authors failed to give a clear theoretical explanation of this effect. After that, a theoretical concept of a detector was proposed, which is sensitive to different directions of circular and elliptical polarization [28]. In this paper, it is assumed that a two-dimensional electron gas should act as the sensitive part of the detector. However, to date, such detectors have not been implemented in practice.

Summing up all of the above, the development of terahertz technologies is one of the most advanced tasks facing modern science. One of the promising directions in the development of terahertz technology is the use of nanomaterials and low-dimensional structures for the development of terahertz devices. In particular, terahertz field-effect transistors (TeraFET) based on graphene and

carbon nanotubes have already shown themselves well as sensitive, fast, and low-noise terahertz detectors. However, to date, there are no terahertz detectors based on nanocarbon materials sensitive to the polarization and phase of the incident radiation. Such detectors can be extremely useful in solving various applied problems discussed above: terahertz spectroscopy, ellipsometry and holography; telecommunications, security, imaging, and so on.

Thus, the creation and experimental study of terahertz detectors based on graphene and carbon nanotubes for polarization-sensitive detection of THz radiation is of **current interest**.

State of the art

The first mention of experiments on polarization-sensitive detection of terahertz radiation dates back to 1998 [29]. The authors experimentally observed the dependence of the photocurrent on the linear polarization of radiation in dipole receivers based on silicon implanted with oxygen ions on a sapphire substrate. The main result in this work is the fact that the photocurrent in response to radiation polarized perpendicular to the antenna arms exceeded the photocurrent in response to radiation polarized parallel to the antenna arms by a factor of 3–4 (Fig. 2(a, b)). The effect is explained by the different spatial distribution of photoexcited carriers in the semiconductor in response to radiation of different polarizations.

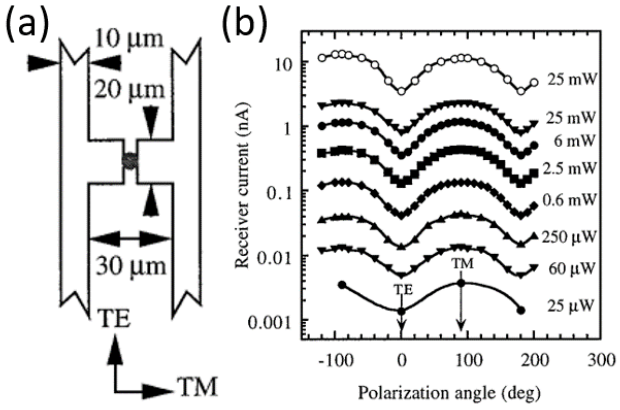

Figure 2 – (a) Schematic diagram of the construction of a dipole terahertz silicon receiver on a sapphire substrate. (b) Dependence of the receiver

photocurrent on the angle of the field of view at a voltage of 28 V, under the influence of voltage, on the value of different voltage power [29].

A similar THz receiver design was proposed in 2005 [30] and then developed in 2007 [31]. Enrique Kstro-Camus et al. used an indium phosphide (InP) substrate doped with iron ions Fe+ by ion implantation. The authors proposed to use a three-contact configuration, in which one common electrode participates in radiation matching with two other, independent electrodes. The proposed receiver made it possible to obtain complete information about both the amplitude and the polarization of the incident radiation (see Fig. 3).

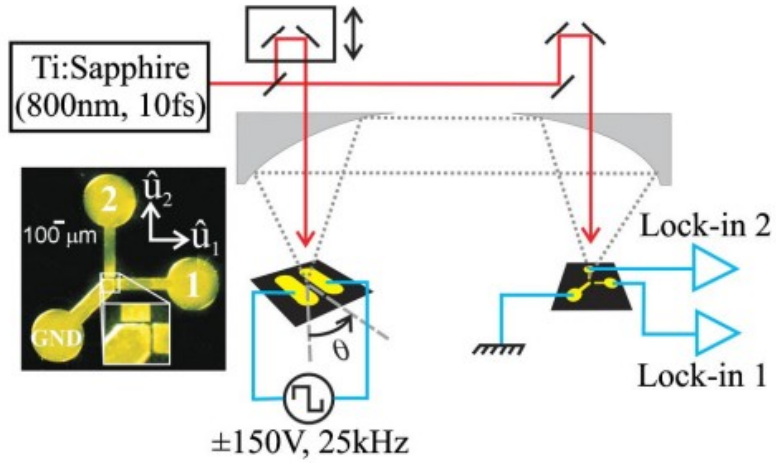

Figure 3 – Optical photograph of a THz receiver based on InP and scheme of the experimental setup [31].

The devices discussed above have demonstrated the ability to distinguish the states of linear polarization of terahertz radiation. However, they had a significant drawback. All of them were made in a dipole configuration, without the possibility of electrical adjustment of the detector operation, which significantly narrowed the possibilities of applied applications of such devices. The first steps to solve this problem were taken in 2008. In several works [32–34], it was proposed to use the so-called field-effect transistors with high electron mobility based on heterostructures. A significant advantage of such devices is the possibility of electrostatic adjustment, using a voltage applied to the gate electrode. This voltage

allows you to control the concentration of charge carriers in the channel of the device, and, as a consequence, its conductivity (impedance).

This makes it possible to maximize the magnitude of the photoresponse and to perform tuning between different operating modes of the device. In [32], a commercial HEMT FUJITSU FHX45X based on a GaAs/AlGaAs heterostructure was studied (Figure 4(a)). The photoresponse of a transistor to radiation from a Hahn diode with a frequency of 100 GHz at room temperature was studied. The dependence of the photovoltage on the angle between the linear polarization of the radiation and the axis of symmetry of the device was measured (Figure 4(b)). The authors assumed that the main mechanism of the response is the straightening of the electron plasma wave, which arises under the action of radiation, on the nonlinearities in the channel. The radiation was coordinated with the device using aluminum wires that connected the transistor terminals with contact pads on the ceramic case, where the test chip was attached.

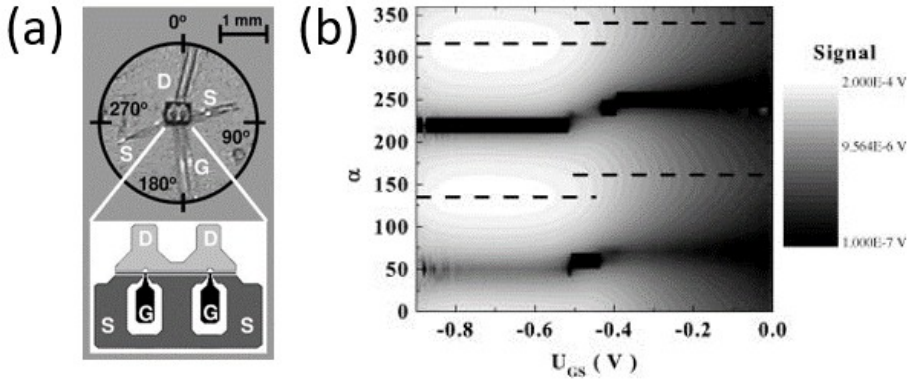

Figure 4 – (a) Schematic representation of HEMT FUJITSU FHX45X based on GaAs/AlGaAs heterostructure. (b) Map of the polarization-dependent part of the photoresponse versus gate voltage and angle α [32].

The authors managed to establish that the dependence of the photoresponse on the linear polarization of radiation is π-periodic and is described by a simple phenomenological formula in which the photovoltage S is proportional to cos 2(α), where α - is the angle between the axis of symmetry of the device and the direction of polarization.

In the work [34] the authors independently fabricated a MESFET based on the GaAs/AlGaAs/GaAs heterostructure. Also, as in the previous publication, the photoresponse of the device to linearly polarized terahertz radiation at room temperature was studied, but in a wider range of radiation frequencies: 0.14 - 1 THz. In addition, the authors obtained estimates of the noise equivalent power of the detector (NEP - noise equivalent power) for radiation with a frequency 1 THz: $10^{-9}\ W/Hz^{1/2}$; and relaxation time 10 ns. To describe the physical mechanism of DC photocurrent generation, we used the model of bulk plasma wave rectification. It was shown that the dependence of the photoresponse on linear polarization is π-periodic, as in the work [32].

Field-effect transistors based on heterostructures have shown themselves well as a tool for detecting linearly polarized radiation. However, in these works, the detection of radiation with circular and elliptical polarizations was not considered at all. The first attempt to fill this gap in experimental studies was made in 2012. Drexler et al. studied a 2D electron gas heterostructure based on GaAs/AlGaAs [27]. They used a commercial HEMT just like the one at work [32]. The wires connecting the transistor on the chip with contact pads on the holder acted as antennas that matched the radiation with the device channel (Fig. 5(a)). In this work, for the first time, the effect of a reversal of the sign of the DC photovoltage depending on the chirality of circularly polarized radiation was observed (Fig. 5(b)). The result was explained in terms of the generalized Dyakonov-Schur hydrodynamic model, in which the photovoltage arises as a result of the conversion of radiation into two alternating currents interfering with each other, shifted in phase relative to each other, and rectified by the nonlinearity in the device channel. The currents propagated in the transistor channel, one from the source to the drain, and the other from the drain to the source.

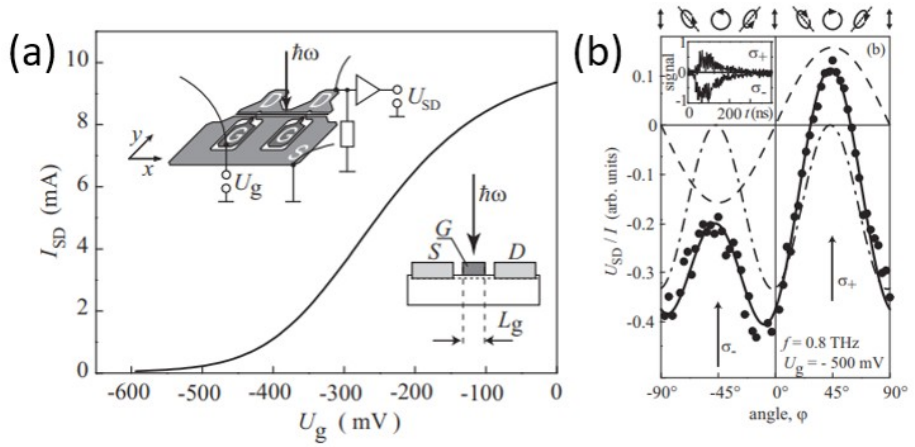

Figure 5 – (a) Transistor characteristic of the device. Top inset: schematic diagram of the device and experiment. On the inset below: a diagram of the side cut of the device. (b) Photovoltage as a function of radiation chirality measured at a frequency of 0.8 THz at room temperature. The dashed and dash-dotted lines show the individual contributions proportional to the parameters U_A and U_B respectively. The ellipses above illustrate the polarization states for various ϕ - phase plate rotation angles $\lambda/4$. The inset shows the photosignal pulses measured for σ^{+} and σ^{-} radiation polarization states [27].

The result was obtained for the radiation frequency f = 0.8 THz, at room temperature, various states of elliptical and circular polarization were achieved by rotating the phase plate $\lambda/4$ in the optical path of the experiment.

The experimental data were approximated using the phenomenological formula:

$$U(\phi)=U_A(U_g,f)\cdot\sin(2\phi)+U_B(U_g,f)\cdot\cos^2(2\phi+\theta)+U_C) \quad (1)$$

where ϕ – is the angle of rotation of the phase plate $\lambda/4$; $U_{A,B}$, U_C and θ – these are adjustment parameters. It follows from this formula that the chiral photoresponse is $\pi/2$-periodic. In contrast to the response to linearly polarized radiation, which is π-periodic.

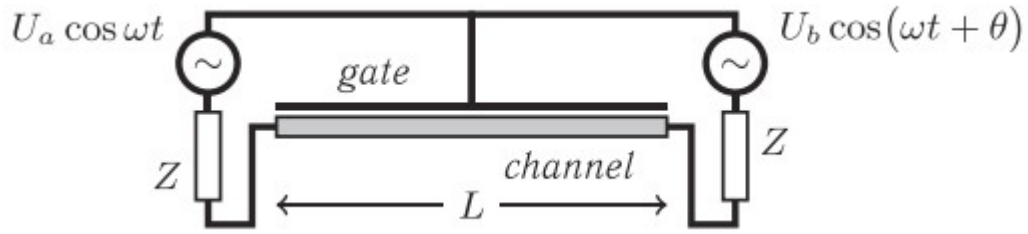

Figure 6 – Schematic representation of the model: antennas are presented in the form of high-frequency alternating current sources [35].

In 2013, Romanov and Dyakonov published an article [35], in which a theoretical model was proposed that describes the experimental results obtained a year earlier in the work of Drexler et al. [27]. The article presented the calculated dependences of the chiral-sensitive part of the photoresponse on such experimental parameters as: antenna impedance, gate electrode length, and gate voltage. The charge carriers in the transistor channel were described using the continuity equation and Ohm's law in differential form:

$$\frac{\partial \rho}{\partial t} + \frac{\partial j}{\partial x} = 0 \tag{2}$$

$$j(x) = -\sigma \frac{\partial U}{\partial x} \tag{3}$$

where ρ and j – specific charge density and current in the channel, respectively, $\sigma = \rho\mu$ – two-dimensional conductivity, μ – charge carrier mobility, $U = V_g - V_{th}$ - gate voltage swing, V_g – gate voltage, V_{th} – threshold voltage.

And the boundary conditions of the problem assumed that the drain and source are sources of alternating current, with the same amplitude, but different phase (see Fig. 6):

$$U_a \cdot \cos(\omega t) - jZ = U_1, \text{ for } x = 0 \tag{4}$$

$$U_b \cdot \cos(\omega t + \theta) + jZ = U_2, \text{ for } x = L \tag{5}$$

where Z – antenna's impedance.

As a result, the solution of equations with given boundary conditions is the following formula for the DC photovoltage:

$$\Delta U = \frac{1}{4} F_0 \cdot \left(U_a^2 - U_b^2 \right) + \frac{1}{2} F_1 U_a U_b \cdot \sin(\theta) \quad (6)$$

The formula includes two terms: the first is proportional to the difference in the squares of the voltages at different ends of the channel, and the second is the product of these voltages by the sine of the phase difference between them. The second term is responsible for the effect of the DC photoresponse sign reversal and current interference within the framework of the proposed model.

In 2015, another implementation of chirally sensitive detection of terahertz radiation was proposed using a high electron mobility transistor (HEMT) based on a heterostructure: InAlAs/InGaAs/InAlAs/InP [36]. The transistor had two gate electrodes G_1 and G_2, made in the form of two periodic lattice-combs inserted one into the other (see Fig. 7(a,b)). This design made it possible to provide a non-uniform periodic distribution of charge carriers in a two-dimensional channel. The sign of the photocurrent in response to radiation of circular polarization changed depending on the distribution of the periodic potential in the structure (see Fig. 7(c,d)). A feature of the work is that the mechanism of chiral-sensitive detection differs from what was considered earlier. Chirally sensitive detection in such a device cannot be described in terms of the Dyakonov-Schur hydrodynamic model. The main mechanism for detecting radiation in such a structure, the authors of the work call the ratchet effect, which is caused by a periodic potential distribution in the channel [37].

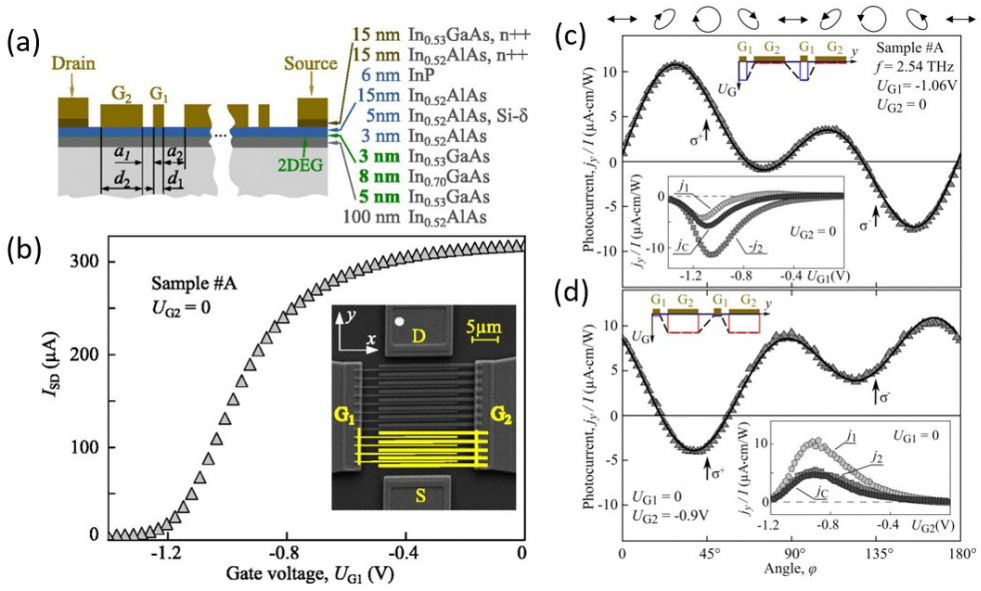

Figure 7 – (a) Sketch of a HEMT with two arrays. The cross section of the structure shows the sequence of layers, the width between the fingers and the width of the fingers. We used THz radiation at a frequency of 2.54 THz at normal incidence. (b) Drain-source current as a function of the gate voltage U_{G1}, at $U_{G2} = 0$ V. The inset shows a photograph of the structure (c, d) Normalized photocurrent induced by terahertz radiation j_y/I as a function of the angle ϕ, which determines the helicity of the radiation. Current is measured at different voltages applied to the first and second gates [36].

From 2018 to 2020, the theory of chirally sensitive photoresponse in field-effect transistors with a two-dimensional electron gas was actively developed in a series of works by Gorbenko, Kacharovsky and Schur [24, 28, 38]. As a result, the authors calculated and proposed various materials and operating modes for TeraFET with 2DEG. The developed theory is an extension of the Dyakonov-Schur model for the case of an asymmetric detector antenna design.

However, the devices described in the works [24, 28, 38] was not created. This work is devoted to the manufacture of such devices and the demonstration of their effective application for polarization- and phase-sensitive detection of THz radiation.

Based on this, **the object** of study is selected: polarization-sensitive detectors based on graphene and carbon nanotubes. And **the goal** and **main objectives** of the study, presented in the introduction, are set.

Goal of the study

Study of the possibilities of creating asymmetric field-effect transistors based on graphene and carbon nanotubes. Study of the physical mechanisms of the polarization-sensitive photoresponse that occurs in such structures under the action of terahertz radiation.

Research objectives

1. Produce several batches of field-effect transistors of different geometry and configuration based on graphene and carbon nanotubes.

2. Experimentally investigate the interaction of circularly polarized terahertz radiation with asymmetric field-effect transistors based on graphene and carbon nanotubes.

3. Confirm experimentally that the DC voltage signal arising in devices under the action of terahertz radiation has a different value for right and left circular polarization at different temperatures and radiation frequencies.

4. Investigate electron transport at low temperatures in transistors with contact asymmetry.

5. Experimentally demonstrate that the tunnel contact can be used for spectroscopy of single-particle states and measurement of the band gap in carbon nanotubes.

Basic research methods

Carbon nanotubes synthesis methods

The substrate, on which the catalytic particles are preliminarily deposited, is placed in a chemical reactor. There, in the flow of reacting and buffer gases, a film of the required substance is formed on the surface of the substrate as a reaction

product of the reacting gas and catalytic particles. The gaseous reaction products are carried out of the reactor chamber in the gas stream. In the framework of this work, a three-component suspension was used as a catalyst $Fe(NO_3)_3 - MoO_2 - Al_2O_3$ in isopropyl alcohol, in the ratio: $10 - 1 - 2$, with concentration $C_{MoO_2} = 1.5$ μg/ml. Methane was used as the carbonaceous gas (CH_4), and hydrogen as a buffer gas (H_2). The reactor was cleaned before synthesis and the substrate was cooled after synthesis in an argon flow (Ar). The scheme of the experiment on the CVD−synthesis of carbon nanotubes is shown in Figure 8. Catalytic metal particles sorb and dissolve carbon-containing gas molecules under the action of high temperature. After that, carbon atoms diffuse into the catalytic particle, reach supersaturation and deposit on the surface of the nanoparticle, forming the walls of the carbon nanotube. An important step in the synthesis process is the preparation and application of catalytic particles. The catalyst suspension was subjected to ultrasonication for 4-6 hours before being applied to the substrate to destroy large particle agglomerations and uniform mixing. Using a microdoser, 60 μl of the suspension was applied to the substrate. After that, the suspension was evenly distributed over the surface by centrifugation at a speed of 3000 rpm for 60 seconds. The specific parameters of all stages of synthesis: the concentration of the suspension and the ratio of components in it, the temperature of synthesis, the time of synthesis and cooling, the ratio of gas concentrations, etc., were selected experimentally, taking into account the results of previous works that used the same technological process [39,40]. A table with the exact parameters of all stages of the synthesis is presented in the appendix. The main disadvantage of the method is that it is impossible to predict in advance exactly where carbon nanotubes will end up on the substrate. This fact complicates the process of manufacturing devices from such randomly arranged tubes.

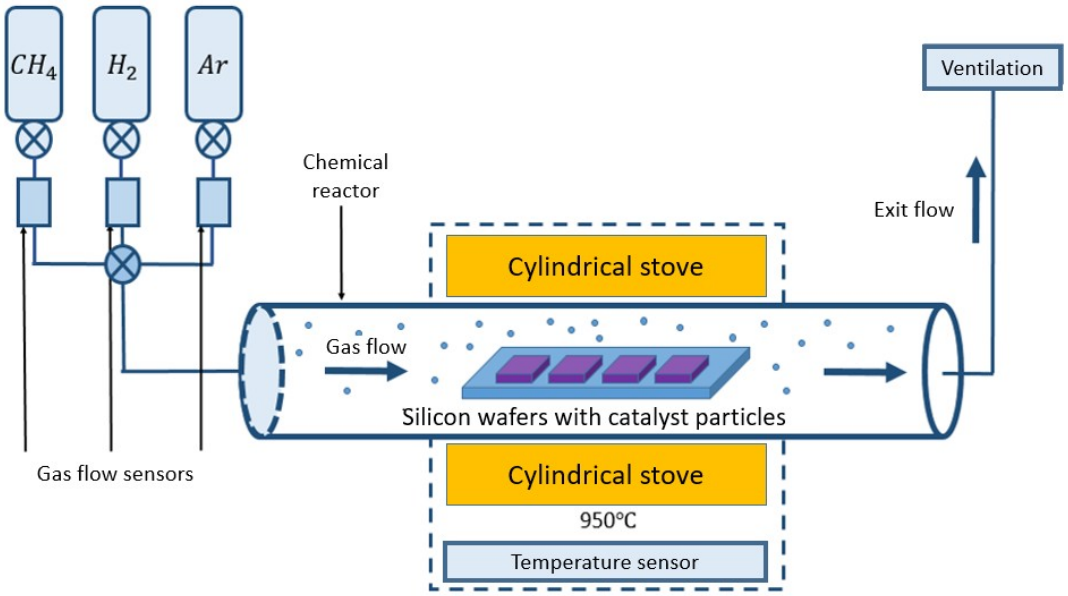

Figure 8 — Scheme of the experimental setup for CVD synthesis of carbon nanotubes.

Graphene synthesis methods

The method is based on the fact that heated metal (Ni, Cu, Ir) surface absorbs carbon-containing gas molecules (CH_4, CO_2). At the same time, carbon atoms remain on the surface, while other atoms that make up the gas molecules pass into a vapor state. With the right selection of process parameters, a graphene film is formed on the metal surface. The choice of this method is justified by the fact that, on the one hand, it makes it possible to obtain sufficiently high-quality films with mobility up to 10000 cm^2/V·s at room temperature, on the other hand, it is quite technologically advanced and makes it possible to relatively quickly and cheaply obtain homogeneous graphene films with an area of several square centimeters [41].

The synthesis process took place in several stages in a chemical reactor (Fig. 9(a)). First, copper foil was annealed in a gas mixture $Ar : H_2 = 4 : 1$ at a pressure of 500 mbar. The annealing process was carried out at a temperature 840 $℃$ within 20 minutes. Then the camera was fed CH_4 portion of 7 mbar. The synthesis of the graphene film continued for 20 minutes. After that, the copper foil was very

quickly cooled to room temperature, within 10 seconds. The most important synthesis parameter is the relative percentage of methane and the rate of its supply. Methane was pumped into the chamber at a flow rate 280 cm^3/min within 6 seconds. A change in methane consumption leads to the formation of graphene films of different thicknesses containing different amounts of defects [42]. The synthesis process is shown schematically in Figure 2.5(b). After synthesis, graphene from copper foil was transferred to a substrate Si/SiO_2 the so-called "wet" method. A diagram of the transfer process is shown in Figure 9(c). Graphene was coated with polymethyl methacrylate (PMMA) using the centrifugation method, after which copper was etched in sodium presulfate.

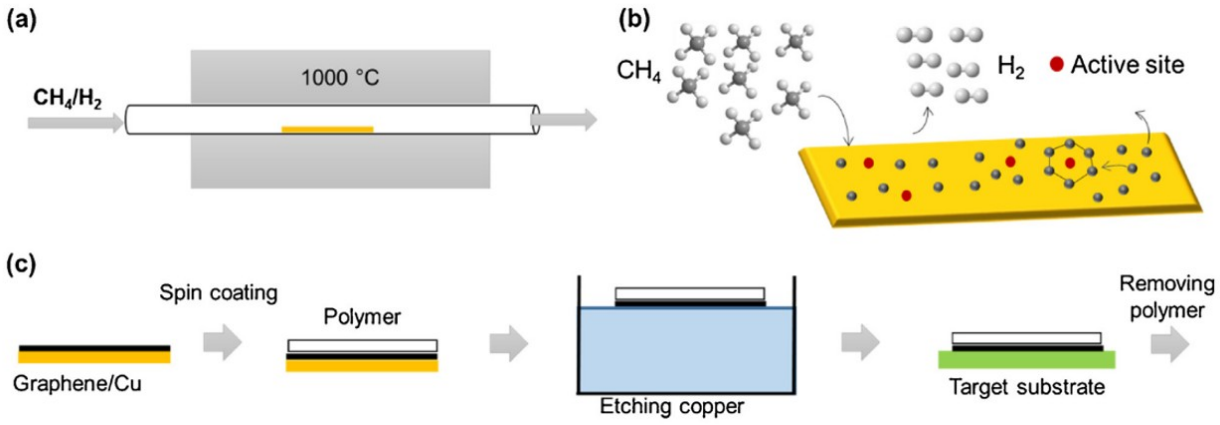

Figure 9 — Synthesis and transfer of graphene. (a) Diagram of a chemical reactor. (b) Illustration of graphene film growth. (c) Scheme of graphene transfer from copper foil to the substrate [43].

Then, the PMMA-coated graphene was transferred to the substrate, and the resist was removed from the graphene surface with acetone. As a result of synthesis, both individual grains of single-layer graphene and a continuous film covering the entire surface of the substrate can be obtained.

Field effect transistors creation methods

Field-effect transistors based on both graphene and carbon nanotubes were fabricated on oxidized silicon substrates Si/SiO_2 grade KDB-12 (100) with a resistivity of 10 Ohm cm at room temperature. The choice of this silicon is due to

the fact that, due to its low conductivity, it is partially transparent to THz radiation. The thickness of Si was 480 μm, and the thickness SiO_2 - 500 nm. At the first stage of the technological route, small areas of graphene, blanks of future transistor channels, were etched using electron lithography through a 950PMMA A4 electron resist mask in oxygen plasma (Fig. 10(1-3)). At the next step, contact interfaces were made to small pieces of graphene: electron lithography was carried out on a two-layer resist (MMA EL6 and 950PMMA A4), after which gold was deposited - 25 nm (Fig. 10(4-6)). Further, also through a mask of a two-layer resist, electron-beam deposition of aluminum oxide was carried out. Al_2O_3 - 100 nm (Fig. 10(7-9)), thus the graphene channel was encapsulated in a dielectric, which protected it from subsequent contamination arising during the technological process. The main function of aluminum oxide is that it acts as a gate dielectric. In addition, aluminum oxide on the surface of graphene reduces the level of its chemical doping to almost zero [44]. This point requires a separate explanation. Graphene free lying on the substrate is strongly oxidized, becomes p-doped, and because of this, it is necessary to apply high values of the gate voltage in order to bring the position of the Fermi level close to the electrical neutrality point of graphene. Aluminum oxide helps to avoid this problem. At the next stage, the upper gate electrode was made using electron lithography and electron beam deposition of Ti-Au 5-200 nm (Fig. 10(10-11)). Then, all excess graphene was etched from the substrate in oxygen plasma (Fig. 10(12)). At the last stage, using laser lithography and thermal vacuum evaporation of Ti-Au 5 100 nm, bow-tie antenna sleeves and large contact pads were fabricated (Fig. 10(13-15)), to match graphene with radiation and connect it to contacts on case.

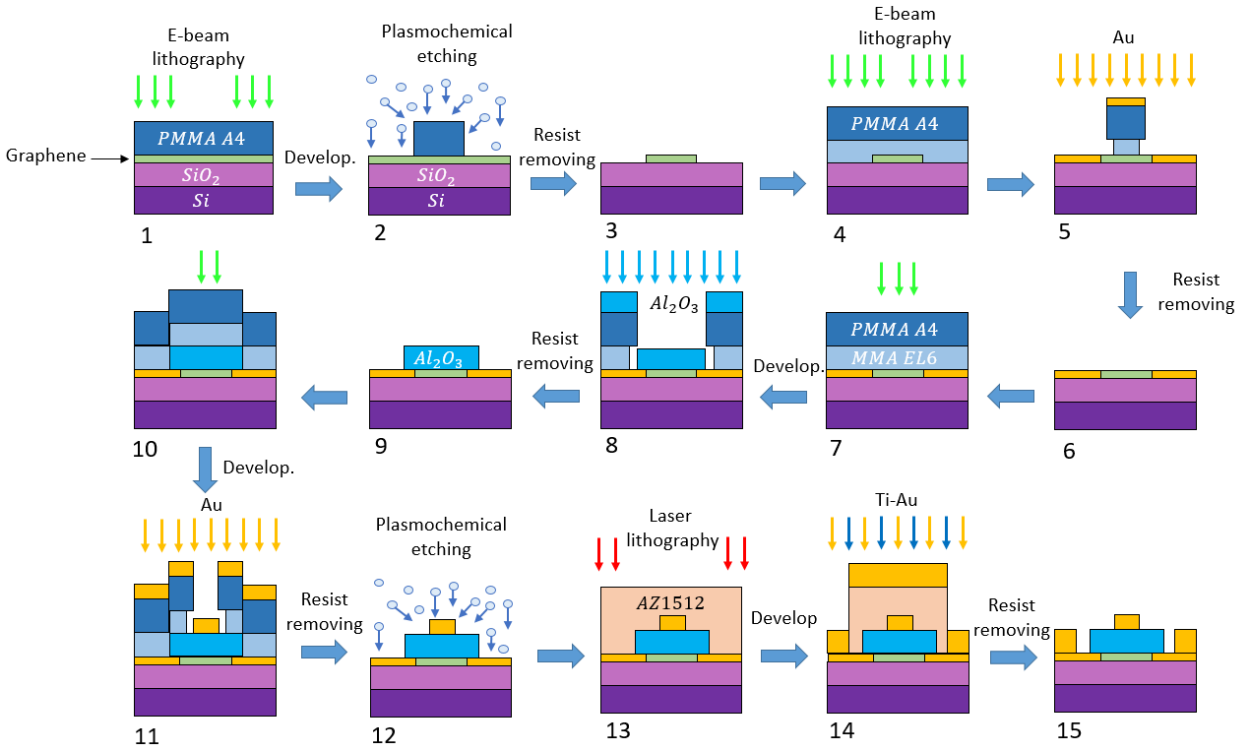

Figure 10 — Technological route for the manufacture of a field-effect transistor based on graphene.

Photoresponse measurement

Experiments on the interaction of the samples studied in the work with terahertz radiation were carried out on an experimental stand, the scheme of which is shown in Fig. 11. A constant methanol vapor laser could operate at two radiation frequencies with two different powers. Immediately after the exit from the laser, an optomechanical beam chopper was installed, which was connected to the reference input of the synchronous detector (Lock-In SR830). An optomechanical chopper modulated the radiation at a low frequency of 77 Hz. Then, the polarization of the radiation was transformed using phase plates $\lambda/2$ (in the experiment with the rotation of linear polarization) and $\lambda/4$ (in the experiment with the transformation of linear polarization into elliptical). After that, the optical path of radiation was divided into two, using a beam splitter. Half of the radiation went to a pyroelectric detector, which measured the radiation power. And the other half, reflected from two parabolic mirrors, was wound up in the window of an optical cryostat. The sample was installed in a cryostat on a special mechanical holder at the end of a

long insert. The cryostat insert was equipped with a resistive oven and a temperature sensor. Cooling was carried out by continuously pumping helium vapor through the volume of the cryostat. Regulation of the intensity of the helium flow and the heating power of the stove made it possible to work at any point in temperature in the range from 4.2 to 300K. In the experiment, we measured the constant voltage that appeared between the drain and source electrodes of the sample under the influence of terahertz radiation. This voltage was measured with the A-channel of a synchronous detector at a reference modulation frequency of 77 Hz. The dependence of the photovoltage on the gate voltage was measured at a fixed polarization and temperature, or the dependence of the photovoltage on the angle of rotation of the phase plate, at a fixed value of the gate voltage and temperature. Similar sets of measurements were carried out at different temperatures.

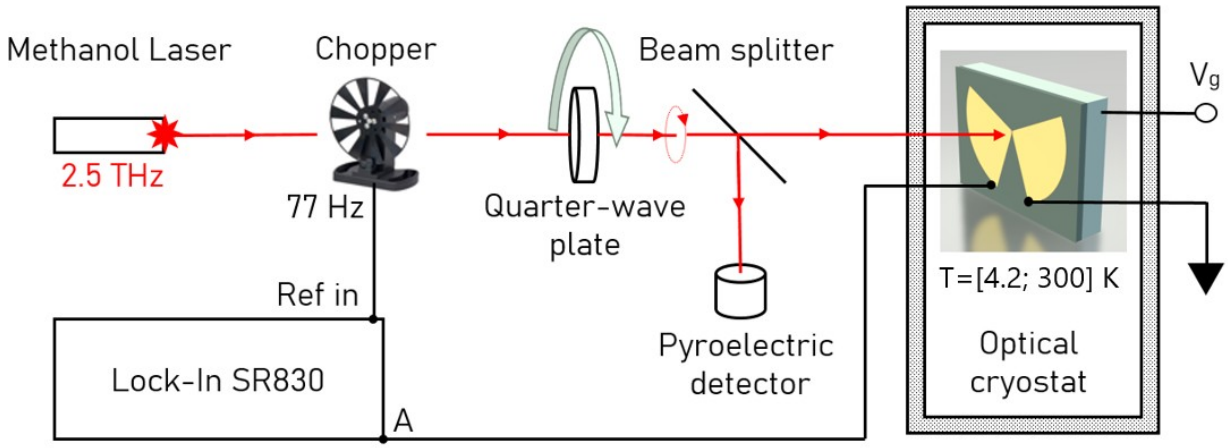

Figure 11 — Scheme of the experimental setup for experiments on synchronous detection of THz radiation.

Tunneling spectroscopy

Tunneling spectroscopy is a method for studying the electronic structure and energy levels of materials based on electron tunneling through a potential barrier. It is based on the phenomenon of quantum tunneling, in which electrons can penetrate a potential barrier that has insufficient energy for their direct penetration. Tunneling spectroscopy uses tunnel contacts, which are structures consisting of

two conductors separated by a thin insulator or vacuum. In the presence of a potential difference between the conductors, electrons from one conductor can "tunnel" through the insulator and enter the other conductor. The dependence of current on voltage between conductors is called the tunnel characteristic. Tunneling spectroscopy makes it possible to study the energy levels of materials and their electronic structure. By measuring the tunneling characteristic at different stress values, it is possible to obtain a spectrum of energy states, that is, information about the allowed energy levels and the density of states of the material. Tunneling characteristics were measured using Stanford Research 570 commercial current amplifier. Drain-source voltage (V_{sd}) and source-gate (V_g) applied from the analog outputs of the National Instruments (NI) data acquisition card. The current was also measured using the NI data acquisition card (Figure 12). The differential conductivity was obtained by numerical differentiation of the current-voltage characteristics. Measurements at low temperatures and high magnetic fields were performed in a CFMS-16 cryogenic system.

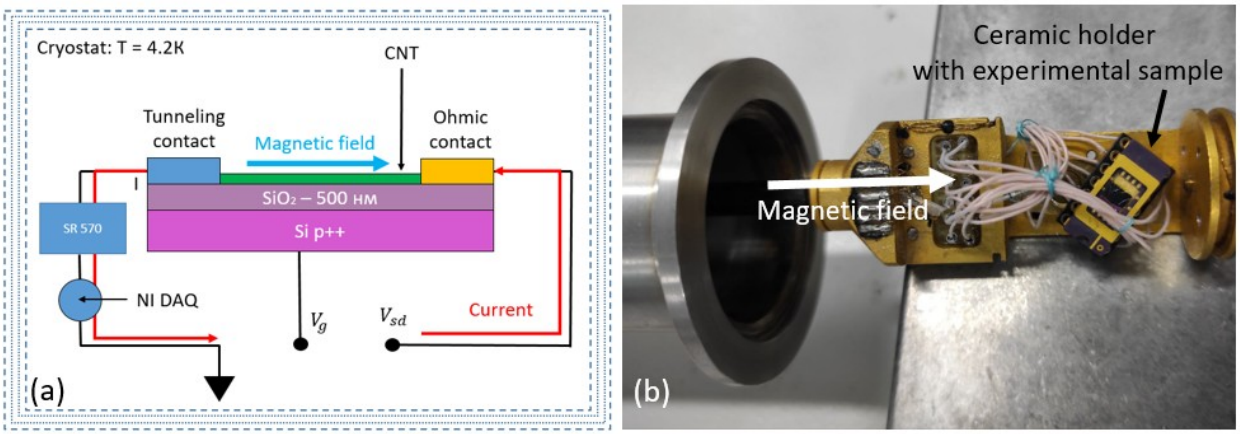

Figure 12 — (a) Schematic diagram of the experiment. (b) Photograph of a cryostat insert with sample mounted on a ceramic holder.

Main results

In the course of performing the tasks set in the work, three types of field-effect transistors based on graphene and carbon nanotubes were manufactured (Figure 13):

• (i) Geometrically asymmetric graphene-based transistors (devices D1, D2);

• (ii) Transistors based on carbon nanotubes with geometric asymmetries (device D3);

• (iii) Transistors based on carbon nanotubes with contact asymmetries (D4 devices);

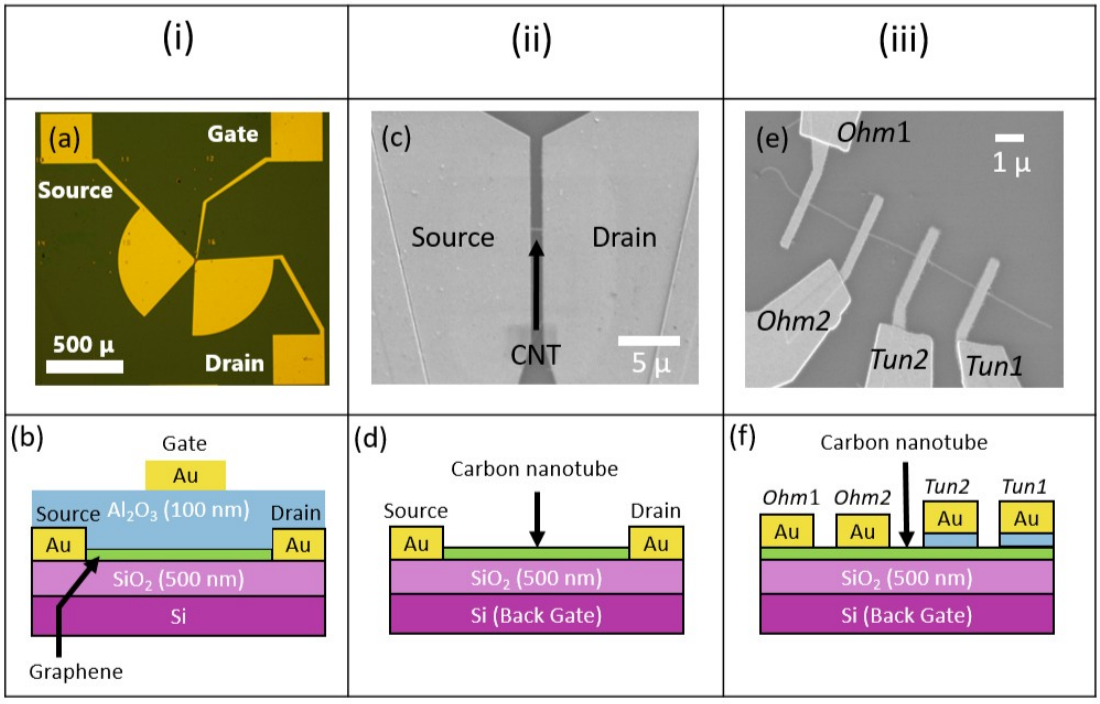

Figure 13 — Diagrams and images of the three types of transistors studied in the work.

Types (i) and (ii) devices were characterized by drain-gate measurements (see Figure 14). Depending on the direction of the gate voltage deployment, a hysteresis typical for such devices was observed. The conductivity minimum corresponds to the point of electrical neutrality in graphene.

From measurements of conductivity versus gate voltage for sample D1, the dissipation time and mobility were estimated based on the Drude model (see Figure 15). The conductivity of graphene is determined by the expression:

$$G=¿¿ \quad (7)$$

where E_F is the Fermi energy, τ is the carrier scattering time in the Drude model, which depends on the energy. The Fermi energy depends on the concentration of charge carriers:

$$E_F=\frac{h}{2\pi}\cdot v_F\sqrt{\pi n} \quad (8)$$

and the concentration of charge carriers in channel n is controlled by the gate voltage:

$$n=\frac{\varepsilon V_g}{4\pi e} \quad (9)$$

where V_g is the gate voltage, which is measured from the Dirac point in graphene, ε is the permittivity of the gate dielectric material, d is its thickness.

The mobility curve shown in Figure 15(c) was obtained using the formula:

$$\mu=\frac{1}{e}\frac{dG}{dn}=\frac{1}{e}\frac{dG}{dV_g}\frac{dV_g}{dn} \quad (10)$$

The attenuation length of the plasma wave was estimated from the formula:

$$L^{¿}=\frac{s\sqrt{2}}{\sqrt{\omega\gamma}} \quad (11)$$

where $\gamma=1/\tau$, and ω is the frequency of the radiation incident on the sample, s is the velocity of the plasma wave, which was estimated by the formula:

$$s=\left[\frac{16\pi^2 e^3 d v_F^2 V_g}{\varepsilon h^2}\right]^{1/4} \quad (11)$$

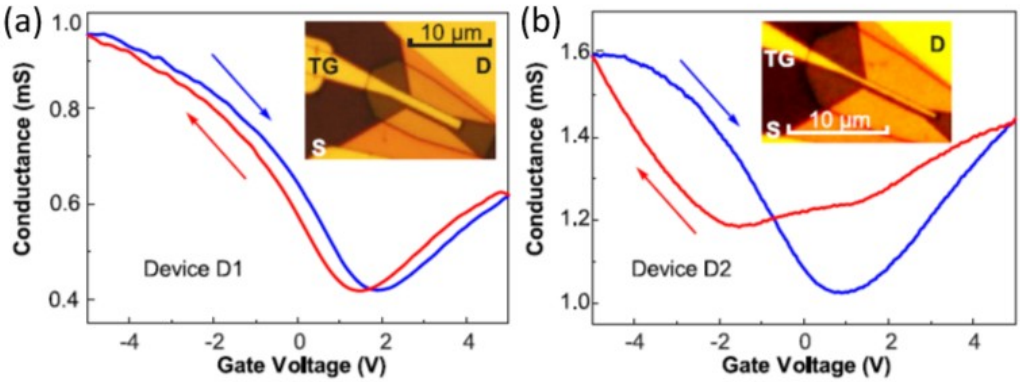

Figure 14 — Dependence of conductivity on gate voltage for graphene-based field-effect transistors with geometric asymmetry.

Estimates of characteristic values based on formulas (7) - (11) for samples D1 and D3 are presented in Table 1.

Table 1. Estimates of the scattering time, mobility, and decay length of a plasma wave for a field-effect transistor based on graphene and a carbon nanotube.

Sample #	τ, fs	$\mu, cm^3/V \cdot s$	L', nm
D1	20	1500	100
D3	100	10000	200

The main results of experiments on the polarization-sensitive detection of terahertz radiation by graphene-based transistors are shown in Figure 16. The scheme of the experimental setup for measuring the photoresponse is presented in the section "Measuring the photoresponse", in Figure 11. Figure 16 shows the dependence of the photoresponse on the angle of rotation of the phase plate λ/4 in the plane perpendicular to the radiation. These are the dependences of the photoresponse on the polarization of the radiation: the polarization states corresponding to the angles of rotation of the phase plate are plotted in the upper part of the graphs.

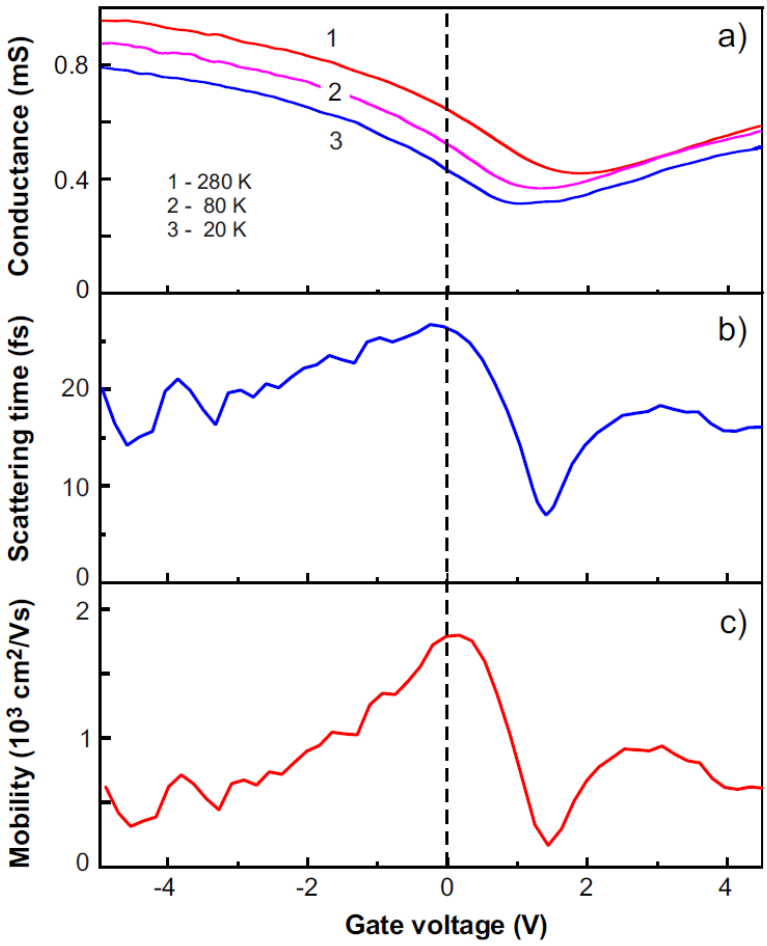

Figure 15 — Analysis of transport properties for device D1 in gate voltage. (a) Conductivity at different temperatures. (b) Scattering time at room temperature. (c) Mobility at room temperature.

The main experimental result for graphene-based samples is the fact that the magnitude of the photoresponse for two different chirality's of circular polarization ($\sigma^{+¿¿}$ - radiation is twisted clockwise when viewed from the source, $\sigma^{-¿¿}$ - counterclockwise) differs by no less than twice. We can say that this is a frequent case of circular dichroism, which is observed due to a combination of two factors: the geometric asymmetry of the antenna, and the use of graphene (2DEG) as a device channel.

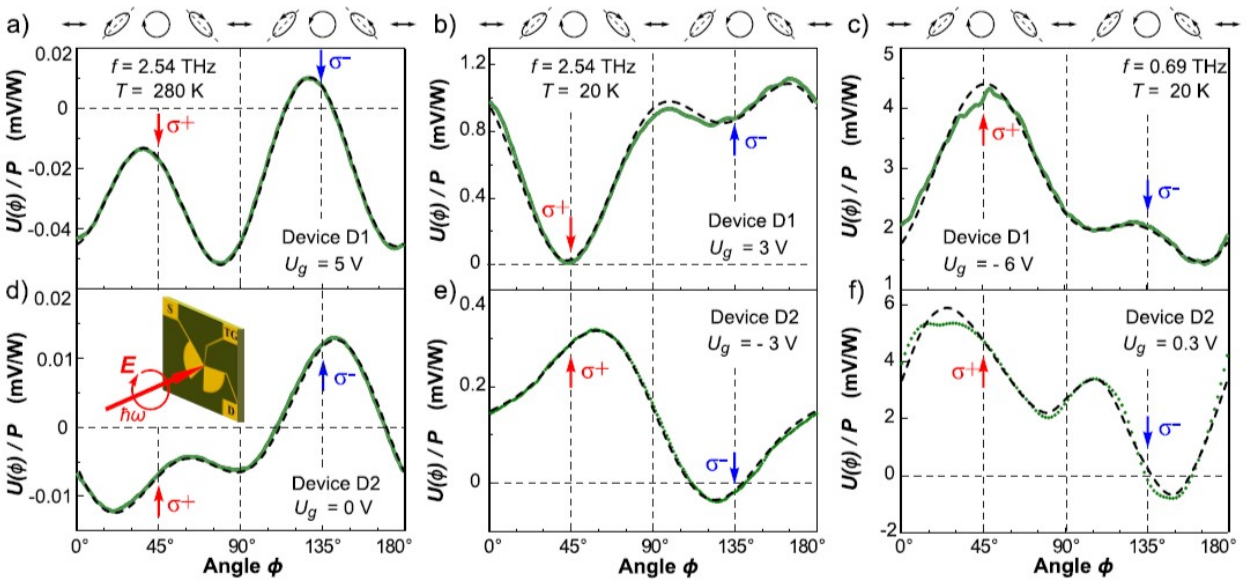

Figure 16 — Dependence of the photoresponse on the angle of rotation of the phase plate λ/4 with respect to the linearly polarized radiation emerging from the laser for two radiation frequencies of 2.54 and 0.69 THz, and two temperatures of 20 and 280 K. Above is the scale of correspondence between polarization directions, and rotation angle values plotted along the x-axis. (a, b, c) top row, results for sample D1, with a channel length of 1 μm. (d, e, f) bottom row, results for sample D2, with a channel length of 1.5 μm.

The most important results for samples of type (iii) presented in Figure 17 were obtained using the technique described in the "Tunneling Spectroscopy" section. Figure 17(b) shows the dependence of the differential conductivity on the drain-to-source voltage measured at 5 K on a carbon nanotube through a tunnel and ohmic contact in the presence of a magnetic field and without it. The main experimental result is the splitting of the density peak in a magnetic field of 16 T (the splitting value is 2.5 mV/T). This effect is associated with the removal of valley degeneracy in a strong magnetic field and was observed for a single carbon nanotube for the first time.

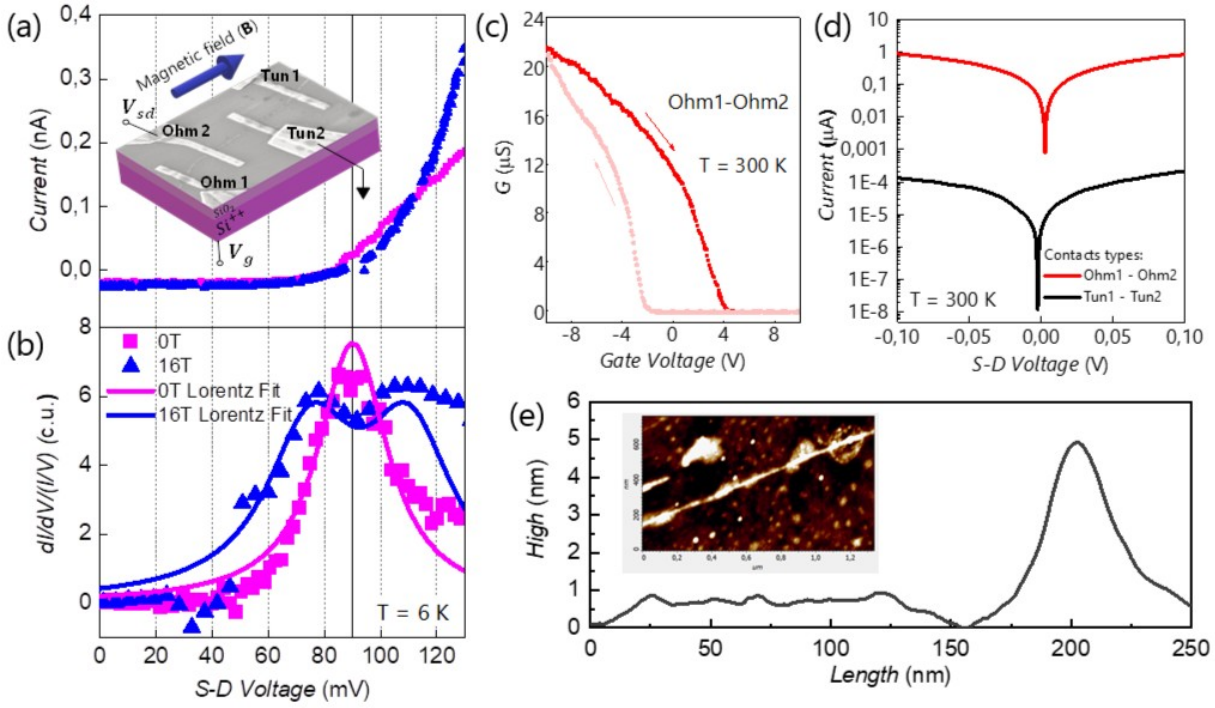

Figure 17 — Device D4. (a) I–V characteristics measured between the ohmic and tunnel contacts in the presence of a magnetic field directed along the tube axis and without it: blue curve (B = 16T) and purple curve (B = 0T). Inset: SEM image of the device with a simple experimental setup. (b) The blue and purple dots represent the I–V curves in Fig. 17(a), numerically differentiated and divided by I/V. The blue and purple lines correspond to the Lorentz function. In a magnetic field B = 16 T, the DOS peak splits into two peaks. The difference in $V_g$units between these peaks is 40 mV. (c) Transistor characteristic of the device: conductance (G) versus gate voltage shows us that the tube is semiconductor (after $V_g > 4$V the conductance is zero). (d) IV measured modulo between two pairs of contacts: Ohm1-Ohm2 and Tun1-Tun2 at room temperature using a probe station. (e) Height profile across the nanotube obtained with AFM. Insert: AFM image of the central part of the device between the contacts Tun2 and Ohm2. The white arrow points to the white line from which the height profile is derived.

Scientific novelty

1. For the first time, the interference of plasma waves in the channel of a field-effect transistor with geometric asymmetry based on graphene and a single carbon nanotube was experimentally observed.

2. Circular effect: different magnitude of photoresponse to circularly polarized radiation twisted clockwise and counterclockwise was first observed in field-effect transistors based on graphene and single carbon nanotubes.

3. It was experimentally shown for the first time that a tunnel contact can be used for spectroscopy of single-particle states and determination of the band gap of single carbon nanotubes.

4. The splitting of the peaks of the density of states of a single carbon nanotube in a magnetic field was experimentally demonstrated.

Basic provisions for defense

1. As a result of rectification of terahertz radiation in the channel of a field-effect transistor with asymmetric geometry, a constant voltage signal is observed, which differs in magnitude by at least two times for right and left circular polarization.

2. The measurement of conductivity versus gate voltage in a field-effect transistor with asymmetric geometry demonstrates a minimum corresponding to the electro neutrality point of graphene and allows us to state that the plasmon attenuation length L* is 100 nm in graphene and 200 nm in carbon nanotube and is comparable to the transistor channel length L = 1 μm, which is a necessary condition for interference.

3. Measurement of the tunneling current, depending on the applied voltage in devices with contact asymmetry, makes it possible to reconstruct the electronic spectrum of single-particle states of a single carbon nanotube and determine its band gap.

4. A magnetic field applied along the axis of a single carbon nanotube in a field-effect transistor with a tunnel contact causes splitting of the peaks in the density of states in its electronic spectrum. This is due to the removal of valley degeneracy under the action of a magnetic field. The splitting value is 2.5 mV/T

Author personal contribution

The author independently obtained all the experimental results presented in this paper, namely:

• performed CVD synthesis of nanocarbon materials: graphene and carbon nanotubes

• characterized, using atomic force and electron microscopy, the synthesized materials

• made field-effect transistors based on these materials using planar technology methods (electronic and photolithography, thin film deposition, plasma-chemical etching, etc.)

• carried out electrical characterization of manufactured devices: measured volt-ampere and gate characteristics

• experimentally measured the photoresponse of finished devices to terahertz radiation and carried out transport measurements at low temperatures

• processed the experimental results

List of published articles on the topic of the dissertation

1. Bogdanova, A.R., Krasnikov, D.V., Khabushev, E.M., Ramirez B, J.A., Matyushkin, Y.E. and Nasibulin, A.G. / Role of Hydrogen in Ethylene-Based Synthesis of Single-Walled Carbon Nanotubes // Nanomaterials. (Q1) – 2023. – T.13. – №.9. – C.1504.

2. Matyushkin, Y., Moskotin, M., Rogov, Y., Kuntsevich, A., Goltsman, G. and Fedorov, G. / Single-particle states spectroscopy in individual carbon nanotubes with an aid of tunneling contacts //Applied Physics Letters. (Q1) – 2022. – T.120. – №.8. – C. 083104.

3. Matyushkin, Y., Danilov, S., Moskotin, M., Fedorov, G., Bochin, A., Gorbenko, I., Kachorovskii, V. and Ganichev, S. / Carbon nanotubes for polarization sensitive terahertz plasmonic interferometry //Optics Express. (Q1) – 2021. – T. 29. – №. 23. – C. 37189-37199.

4. Shabanov, A., Moskotin, M., Belosevich, V., Matyushkin, Y., Rybin, M., Fedorov, G. and Svintsov, D. / Optimal asymmetry of transistor-based terahertz detectors //Applied Physics Letters. (Q1)– 2021. – T. 119. – №. 16. – C. 163505.

5. Matyushkin, Y., Danilov, S., Moskotin, M., Belosevich, V., Kaurova, N., Rybin, M., Obraztsova, E.D., Fedorov, G., Gorbenko, I., Kachorovskii, V. and Ganichev, S. / Helicity-Sensitive Plasmonic Terahertz Interferometer //Nano Letters. (Q1) – 2020. – T. 20. – №. 10. – C. 7296-7303.

Main conclusions

The main results of the work are as follows.

1. Based on the analysis of the literature, the object of study was proposed and the purpose and objectives of this work were formulated.

2. To accomplish the tasks set, technological routes for creating field-effect transistors based on graphene with geometric and contact asymmetry.

3. In the course of the work, the synthesis of nanocarbon materials was carried out: graphene and carbon nanotubes, by chemical vapor deposition.

4. Based on the synthesized materials, 3 experimental batches of field-effect transistors were made:

• based on graphene with geometric asymmetry;

• based on single carbon nanotubes with geometric asymmetry;

• based on single carbon nanotubes with contact asymmetry;

5. It was experimentally shown that transistors with geometric asymmetry make it possible to distinguish the chirality of circularly polarized terahertz radiation from the dependences of the volt-watt sensitivity on the radiation polarization.

6. The chirally sensitive photoresponse was described in terms of the generalized hydrodynamic model of Dyakonov-Schur charge carrier transport. Based on the proposed model, the circular effect in transistors with geometric asymmetry is a consequence of the interference of plasma waves excited in the transistor channel under the action of terahertz radiation.

7. It has been experimentally demonstrated that the tunnel contact in transistors with contact asymmetry is an effective tool for direct measurement of the band gap and density of electronic states of single carbon nanotubes.

The results presented in this paper open up new prospects for the development of terahertz detectors based on nanocarbon materials and plasmon terahertz interferometers sensitive to radiation polarization. Such devices can be in demand in many applied fields. Further research in this direction should be aimed at improving the methods for synthesizing nanocarbon materials and improving the design of detectors.

References

1. The 2017 terahertz science and technology roadmap / S. S. Dhillon [и др.] // Journal of Physics D: Applied Physics. — 2017. — янв. — т. 50, No 4. — с. 043001.
2. Exter M. van, Fattinger C., Grischkowsky D. Terahertz time-domain spectroscopy of water vapor // Optics Letters. — 1989. — окт. — т. 14, No 20. — с. 1128.
3. Terahertz underdamped vibrational motion governs protein-ligand binding in solution / D. A. Turton [и др.] // Nature Communications. — 2014. — июнь. — т. 5, No 1.
4. Zhang T., Zhang Z., Arnold M. A. Polarizability of Aspirin at Terahertz Frequencies Using Terahertz Time Domain Spectroscopy (THz-TDS) // Applied Spectroscopy. — 2018. — дек. — т. 73, No 3. — с. 253—260.
5. Nuss M. C., Orenstein J. Terahertz time-domain spectroscopy // Topics in Applied Physics. — Springer Berlin Heidelberg. —2007— сен. — с. 7—50.
6. Industrial applications of THz systems / S. Wietzke [и др.] // SPIE Proceedings / под ред. X.-C. Zhang [и др.]. — SPIE, 07.2009.
7. Appleby R., Anderton R. N. Millimeter-Wave and Submillimeter-Wave Imaging for Security and Surveillance // Proceedings of the IEEE. — 2007. — авг. — т. 95, No 8. — с. 1683—1690.
8. Ahi K., Anwar M. Advanced terahertz techniques for quality control and counterfeit detection // SPIE Proceedings / под ред. M. F. Anwar, T. W. Crowe, T. Manzur. — SPIE, 05.2016.
9. Variable-wavelength frequency-domain terahertz ellipsometry / T. Hofmann [и др.] // Review of Scientific Instruments. — 2010. — февр. — т. 81, No 2. — с. 023101.
10. Reflective chiral meta-holography: multiplexing holograms for circularly polarized waves / Q. Wang [и др.] // Light: Science & Applications. — 2018. — июнь. — т. 7, No 1.

11. Groppi C. E., Kawamura J. H. Coherent Detector Arrays for Terahertz Astrophysics Applications // IEEE Transactions on Terahertz Science and Technology. — 2011. — сент. — т. 1, No 1. — с. 85—96.
12. A 1.3-THz Balanced Waveguide HEB Mixer for the APEX Telescope / D. Meledin [и др.] // IEEE Transactions on Microwave Theory and Techniques. — 2009. — янв. — т. 57, No 1. — с. 89—98.
13. THz Astrophysics from Dome A / N. Tothill [и др.] // EAS Publications Series. — 2009. — дек. — т. 40. — с. 275—280.
14. Low Noise 1 THz–1.4 THz Mixers Using Nb/Al-AlN/NbTiN SIS Junctions/
A. Karpov [и др.] // IEEE Transactions on Applied Superconductivity. — 2007. — июнь. — т. 17, No 2. — с. 343—346.
15. Millimetron—a large Russian-European submillimeter space observatory /W. Wild [и др.] // Experimental Astronomy. — 2008. — июль. — т. 23, No 1. — с. 221—244.
16. Volume of data/information created, captured, copied, and consumed worldwide from 2010 to 2025. — 03.2022. https://www.statista.com/statistics/871513/worldwide-data-created/.
17. Wireless Communications and Applications Above 100 GHz: Opportunities and Challenges for 6G and Beyond / T. S. Rappaport [и др.] // IEEE Access. — 2019. — т. 7. — с. 78729—7875.
18. The Roadmap to 6G: AI Empowered Wireless Networks / K. B. Letaief [и др.] // IEEE Communications Magazine. — 2019. — авг. — т. 57, No 8. — с. 84—90.
19. Photodetectors based on graphene, other two-dimensional materials and hybrid systems / F. L. Koppens [и др.] // Nature Nanotechnology. — 2014. — окт. — т. 9, No 10. — с. 780—793.
20. Dyakonov M., Shur M. Shallow water analogy for a ballistic field effect transistor: New mechanism of plasma wave generation by dc current //

Physical Review Letters. — 1993. — окт. — т. 71, No 15. — с. 2465—2468.

21. Dyakonov M., Shur M. Detection, mixing, and frequency multiplication of terahertz radiation by two-dimensional electronic fluid // IEEE Transactions on Electron Devices. — 1996. — март. — т. 43, No 3. — с. 380—387.
22. Muravev V. M., Kukushkin I. V. Plasmonic detector/spectrometer of subterahertz radiation based on two-dimensional electron system with embedded defect // Applied Physics Letters. — 2012. — февр. — т. 100, No 8. — с. 082102.
23. Resonant terahertz detection using graphene plasmons / D. A. Bandurin [и др.] // Nature Communications. — 2018. — дек. — т. 9, No 1.
24. Gorbenko I. V., Kachorovskii V. Y., Shur M. S. Plasmonic Helicity-Driven Detector of Terahertz Radiation // physica status solidi (RRL) – Rapid Research Letters. — 2018. — дек. — т. 13, No 3. — с. 1800464.
25. Graphene field-effect transistors as room-temperature terahertz detectors / L.
Vicarelli [и др.] // Nature Materials. — 2012. — сент. — т. 11, No 10. — с. 865—871.
26. Ultrafast graphene-based broadband THz detector / M. Mittendorff [и др.] //
Applied Physics Letters. — 2013. — июль. — т. 103, No 2. — с. 021113.
27. Helicity sensitive terahertz radiation detection by field effect transistors / C. Drexler [и др.] // Journal of Applied Physics. — 2012. — июнь. — т. 111, No 12. — с. 12450.
28. Gorbenko I. V., Kachorovskii V. Y., Shur M. Terahertz plasmonic detector controlled by phase asymmetry // Optics Express. — 2019. — февр. — т. 27,
No 4. — с. 4004.

29. Polarization-dependent efficiency of photoconducting THz transmitters and receivers / P. Huggard [и др.] // Applied physics letters. — 1998. — т. 72, No 17. — с. 2069—2071.
30. Polarization-sensitive terahertz detection by multicontact photoconductive receivers / E. Castro-Camus [и др.] // Applied Physics Letters. — 2005. — июнь. — т. 86, No 25. — с. 254102.
31. An ion-implanted InP receiver for polarization resolved terahertz spectroscopy / E. Castro-Camus [и др.] // Optics Express. — 2007. — т. 15, No 11. — с. 7047.
32. Polarization sensitive detection of 100 GHz radiation by high mobility field
effect transistors / M. Sakowicz [и др.] // Journal of Applied Physics. — 2008. — т. 104, No 2. — с. 024519.
33. Room temperature terahertz detection based on bulk plasmons in antenna coupled GaAs field effect transistors / S. Kim [и др.] // Applied Physics Letters. — 2008. — т. 92, No 25. — с. 253508.
34. Plasma wave oscillations in nanometer field effect transistors for terahertz detection and emission / W. Knap [и др.] // Journal of Physics: Condensed Matter. — 2008. — т. 20, No 38. — с. 384205.
35. Romanov K. S., Dyakonov M. I. Theory of helicity-sensitive terahertz radiation detection by field effect transistors // Applied Physics Letters. — 2013. — апр. — т. 102, No 15. — с. 153502.
36. Helicity sensitive terahertz radiation detection by dual-grating-gate high electron mobility transistors / P. Faltermeier [и др.] // Journal of Applied Physics. — 2015. — авг. — т. 118, No 8. — с. 084301.
37. Nalitov A., Golub L., Ivchenko E. Ratchet effects in two-dimensional systems with a lateral periodic potential // Physical Review B. — 2012. — т. 86, No 11. — с. 115301.

38. Gorbenko I., Kachorovsky V. Y., Shur M. Plasmonic polarization-sensitive detector of terahertz radiation // Journal of Physics: Conference Series. т. 1236. — IOP Publishing. 2019. — с. 012029.
39. Synthesis of individual single-walled carbon nanotubes on patterned silicon wafers / J. Kong [и др.] // Nature. — 1998. — окт. — т. 395, No 6705. — с. 878—88.
40. Synthesis of single-walled carbon nanotubes produced using a three layer Al/Fe/Mo metal catalyst and their field emission properties / Y. Chen [и др.] // Carbon. — 2007. — дек. — т. 45, No 15. — с. 3007—3014.
41. High Quality Monolayer Graphene Synthesized by Resistive Heating Cold Wall Chemical Vapor Deposition / T. H. Bointon [и др.] // Advanced Materials. — 2015. — июнь. — т. 27, No 28. — с. 4200—4206.
42. Efficient nitrogen doping of graphene by plasma treatment / M. Rybin [и др.] // Carbon. — 2016. — янв. — т. 96. — с. 196—202.
43. Emerging trends in 2D nanotechnology that are redefining our understanding
of “Nanocomposites” / P. Liu [и др.] // Nano Today. — 2018. — авг. — т. 21. — с. 18—40.
44. Mechanism of the effects of low temperature Al2O3 passivation on graphene
field effect transistors / C. G. Kang [и др.] // Carbon. — 2013. — март. — т. 53. — с. 182—187.